This document is the accepted manuscript version of the following article:
Matter, M., Nenoff, L., Marc, L., Weber, D. C., Lomax, A. J., & Albertini, F. (2020). Update on yesterday's dose – use of delivery log-files for daily adaptive proton therapy (DAPT). Physics in Medicine and Biology.
https://doi.org/10.1088/1361-6560/ab9f5e

Update on yesterday's dose – Use of delivery log-files for daily adaptive proton therapy (DAPT)

M Matter[1,2], L Nenoff[1,2], L Marc[3], D C Weber[1,4,5], A J Lomax[1,2], F Albertini[1]

[1]Paul Scherrer Institute, Center for Proton Therapy, Villigen, Switzerland, [2]Department of Physics, ETH Zurich, Switzerland, [3]Department of Physics, EPF Lausanne, Switzerland, [4]Department of Radiation Oncology, University Hospital Zurich, Switzerland, [5]Department of Radiation Oncology, University Hospital Bern, Switzerland

Keywords: daily adaptive proton therapy, machine log-files

In daily adaptive proton therapy (DAPT), the treatment plan is re-optimized on a daily basis. It is a straightforward idea to incorporate information from the previous deliveries during the optimization to refine this daily proton delivery. A feedback signal was used to correct for delivery errors and errors from an inaccurate dose calculation used for plan optimization. This feedback signal consisted of a dose distribution calculated with a Monte Carlo algorithm and was based on the spot delivery information from the previous deliveries in the form of log-files. We therefore called the method **U**pdate On **Y**esterday's **D**ose (UYD). The UYD method was first tested with a simulated DAPT treatment and second with dose measurements using an anthropomorphic phantom. For both, the simulations and the measurements, a better agreement between the delivered and the intended dose distribution could be observed using UYD. Gamma pass rates (1%/1mm) increased from around 75% to above 90%, when applying the closed-loop correction for the simulations, as well as the measurements. For a DAPT treatment, positioning errors or anatomical changes are incorporated during the optimization and therefore are less dominant in the overall dose uncertainty. Hence, the relevance of algorithm or delivery machine errors even increases compared to standard therapy. The closed-loop process described here is a method to correct for these errors, and potentially further improve DAPT.

1 Introduction

The concept of adaptive radiation therapy was first introduced by Yan et al. (Yan *et al.*, 1997) as a closed-loop process where the adapted treatment is modified using a systematic feedback of information from previous deliveries. Since then, the main interest in adaptive therapy for conventional radiotherapy has been typically to correct for inter-fractional changes of the tumor and to reduce the effect of daily positioning errors (Yan *et al.*, 1997) . In addition, for protons, the rationale for adaption is also extended to correcting for changes in tissues and structures surrounding the tumor, which can additionally, and significantly, affect the daily delivered dose distribution even if the tumor volume remains the same (Albertini *et al.*, 2008; Hoffmann *et al.*, 2017; Nenoff *et al.*, 2019). Unfortunately, and until recently, such a closed-loop treatment adaption method found only limited applications in clinical practice (Yan *et al.*, 2000; Nijkamp *et al.*, 2012), mainly because the clinical benefits did not outweigh the effort involved for its execution. However, efficient processes for treatment adaption are now being introduced into the clinic with the introduction of MR-Linacs(Kontaxis *et al.*, 2015; Acharya *et al.*, 2016; Raaymakers *et al.*, 2017) for photons, as well as being investigated for daily adaptive proton therapy (DAPT)(Botas *et al.*, 2018;

Albertini *et al.*, 2020) for protons. The idea of DAPT is that a new treatment plan is optimized daily, based on 3D images (CT, CBCT or MRI) acquired just minutes before treatment start. With such developments, it is now being demonstrated that the clinical benefit of planning directly on the current patient geometry outweighs the plan modification effort (Bohoudi *et al.*, 2017; Nenoff *et al.*, 2020).

DAPT or adaptive MR-Linac treatments, are being introduced primarily to address the problem of positioning uncertainty and inter-fraction anatomical changes. There are however other errors in the process of fractionated radiotherapy that could also benefit from using a daily adaptive paradigm. Two such will be investigated in this work - errors resulting from imprecision in treatment delivery and those resulting from the use of a simplified dose calculation for highly efficient plan adaption (Matter *et al.*, 2019). Indeed, since a new treatment plan anyway needs to be generated for online daily adaption, little additional effort is required to address these issues as part of a closed- loop, adaptive process, a concept that was already proposed in the original paper by Yan et al(Yan *et al.*, 1997). In this work, we call this approach **U**pdate on **Y**esterday's **D**ose (UYD). As envisaged by Yan, this is a closed-loop process, which as a feedback, uses the dose distribution calculated from a log-file Monte Carlo (MC) calculation (Winterhalter, Meier, *et al.*, 2019) obtained during the previous delivery or deliveries. As such, we have conducted simulations of the DAPT treatment process to show the potential benefit of UYD and to demonstrate that the UYD process works over multiple factions. Additionally, we have applied the technique experimentally to an anthropomorphic phantom in order to demonstrate that the simulated benefits from UYD translate to measurable improvements in delivery accuracy. For both, we have also investigated different correction approaches, to ensure that either the delivered single fraction dose, or the dose accumulated over a number of fractions, is as close as possible to the originally planned dose. Finally, in the experimental part, we also separate out the effects of delivery and calculational errors to investigate the effectiveness of DAPT for correcting each of them independently.

2 Material and methods

This work is divided into two parts - a simulation and an experimental study with measurements, the methods of which will be described in the following section. An overview of the adaption strategies, which will be investigated in this work is given in figure 1.

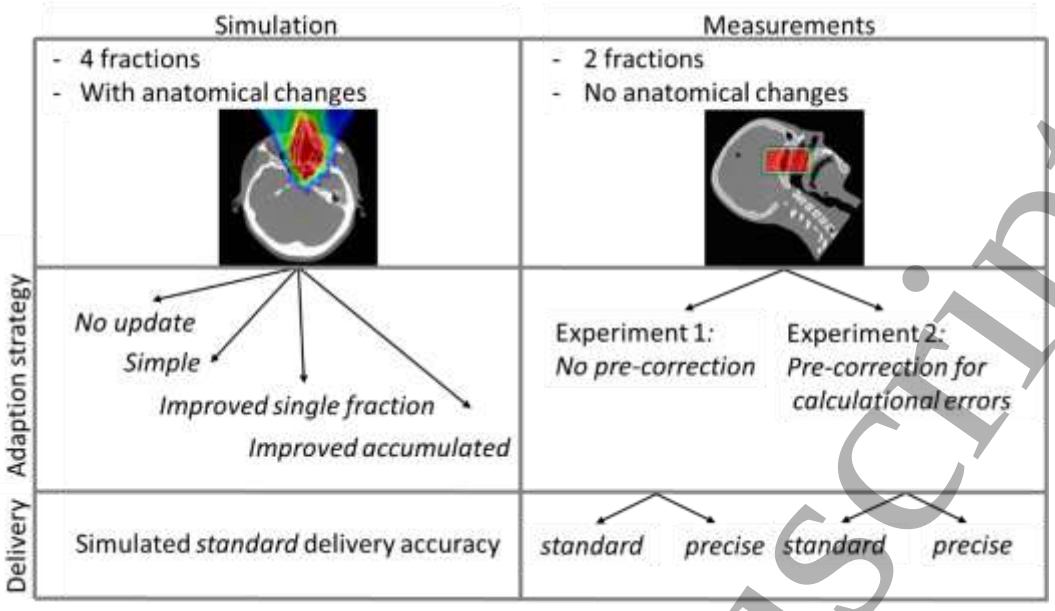

Figure 1 An overview of the different adaption strategies for the Update on Yesterday's Dose (UYD) method.

2.1 Simulations

2.1.1 Simulation study design – The UYD concept

For all simulations, an example clinical case of a tumor in the nasal cavity region has been used (figure 2). In this anatomical region, only very limited organ deformation is expected and therefore a rigid registration for contour propagation and a rigid dose transformation is valid. One planning CT (pCT) and four repeat CTs (CT1 - 4) obtained during an actual patient treatment were available. The repeat CTs were of the same image quality as the planning CT, which for DAPT can be obtained with an in-room CT on-rails (Albertini *et al.*, 2020). We generated a treatment plan with three anterior fields(Nenoff *et al.*, 2019) on the planning CT with our in-house developed TPS. The resulting dose distribution is referred to as target dose (TD). A schematic of the study procedure is displayed in figure 3. For the first fraction, we rigidly *transformed* the TD from the pCT to CT1 (blue arrow). This gave us the TD Fx1. On CT1, we *optimized* a treatment plan, using an ultra-fast, GPU implemented analytical dose calculation and optimization engine (Lomax *et al.*, 1996, Matter *et al.*, 2019). Dose restoration was used to as best as possible approach the TD of Fx1. This generated Plan Fx1 (orange arrow). Finally, we *simulated* an imperfect treatment delivery, by randomly assigning errors to pencil beam positions, and recalculating the Plan Fx1 using a MC algorithm as a 'gold standard' dose calculation (green arrow). This gave us the delivered dose (DD) Fx1, which we transformed back to the pCT for later *dose accumulation*. On the planning CT dose grid, a new TD for the next fraction (the *fraction specific target dose*) was then calculated, taking into account previous delivered doses under different scenarios (see below). The fraction specific target dose is then transformed to the CT of this fraction to guide the adaption for that fraction (purple arrow). We repeated these steps (indicated by the differently colored arrows in figure 3) for all four fractions. Each of these steps is described in more detail in the following sections.

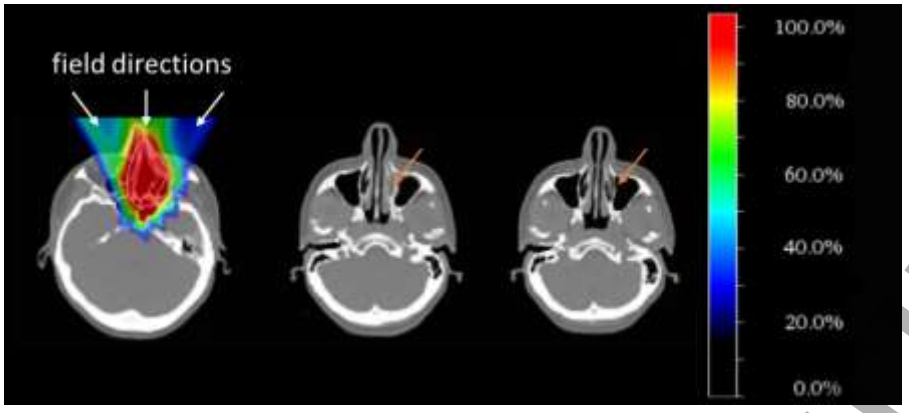

Figure 2 Target dose distribution on planning CT with PTV outlined in white and indicated field incident directions (left) and two repeat CTs (middle and right) with small changes in the nasal cavity fillings indicated with orange arrows. The color wash scale of the dose in % of the prescription is display on the right-hand side of the figure.

Dose transformation

For the rigid *dose transformation*, a rigid registration between the pCT and all repeat CTs was done in Velocity 4.0 (Varian Medical Systems, Palo Alto, CA, USA). The resulting 4x4-transformation matrix, which describes the registration between the CTs, was exported in DICOM. We conducted all rigid dose transformations in our TPS according to these DICOM registration objects.

Daily Plan Optimization

Plan optimization has been performed with an in-house developed TPS using the dose restoration approach (Jagt *et al.*, 2017; Bernatowicz *et al.*, 2018). Dose restoration aims to restore, as much as possible, the initially planned target dose on the new patient geometry. The TPS is based on a ray-casting dose calculation algorithm and a quasi-Newtonian gradient descent optimization algorithm(Lomax *et al.*, 1996), running on a GPU(Matter *et al.*, 2019). The same field arrangement and machine setting (e.g. snout position, iso-center position) were used for every fraction. The weights ω of pencil beam j were optimized as follows:

$$\omega_j(k+1) = \omega_j(k)\frac{\sum_i^{OP} d_{ij}^2 \frac{TD_i^f}{C_i(k)}}{\sum_i^{OP} d_{ij}^2},$$

where k represents the number of optimization iterations and d_{ij} represents the elements of the dose deposition matrix and an optimization point (OP) spacing of 1.75 mm was used. $C_i(k)$ represents the dose at voxel i in iteration k and TD_i^f the target dose of fraction *f*. 200 optimization iterations, which are enough to ensure convergence of the solution, were used for every optimization. The optimization was executed on a GPU, and took less than 20 seconds for full, dose restoring optimization for all cases described in this manuscript.

Delivery simulation

For the *delivery simulation,* two contributions for possible discrepancies between the planned and the delivered dose were considered: machine delivery and dose calculation errors. For the simulation, we recalculated the plans with a MC simulation and added a Gaussian distributed pencil beam position error in both transversal directions (perpendicular to the beam) with a sigma of 0.5

mm. This 0.5 mm sigma approximated the residual positional inaccuracy of the pencil beam position at Gantry 2 at PSI, as will be explained in section 2.2.1. The random transversal spot position error was only a surrogate to estimate real delivery errors, as for this planning study, actual treatment log files were not available. Therefore, we additionally tested the method with real measurements (section 2.2). The MC simulations were performed with TOPAS version 3.0.p1 (Perl *et al.*, 2012) and a scaling of 1000 to reduce calculation time. It was shown that with this scaling a statistical fluctuation of less than 1% can be expected (Winterhalter, Meier, *et al.*, 2019) and a comparison of the MC algorithm with the TPS dose engine is given in (Winterhalter, Zepter, *et al.*, 2019). This simulation with the added error for the pencil beam position emulated the delivered distribution (DD) of the corresponding fractions. The DD were transformed back to the pCT with the inverse transformation matrix, obtained from Velocity.

Dose accumulation

On the pCT, we calculated the accumulated dose (AD) of fraction *f* as follows,

$$AD^f = \frac{1}{f}\sum_{i=1}^{f} DD^i.$$

Fraction specific target dose calculations

Four different strategies for definition of the fraction specific target doses have been investigated: *No update*, *simple*, *improved (accumulated)* and *improved (single fraction)*, as described in the following.

1. *No update*. The initial TD is used as the fraction specific target dose for all fractions.

$$TD^f_{no\ update} = TD$$

2. S*imple.* The fraction specific target dose is calculated by adding the difference of the TD and the AD (up to this fraction).

$$TD^f_{simple} = TD + (TD - AD^{f-1})$$

3. *Improved (accumulated)*. This third strategy was designed to improve the agreement between the AD and the TD. Since no log-file is available to correct the delivery of the first fraction (DD^1), DD^1 displays strong delivery and dose calculation errors. Hence, the AD will only gradually converge towards the TD. In this scenario, the situation can be improved by double correcting for the delivery error of the first fraction ($TD\text{-}DD^1$) to compensate for the first uncorrected delivery.

$$TD^f_{improved\ AD} = TD + (TD - DD^1) + \left(TD - AD^{f-1}\right) = 3 \cdot TD - DD^1 - AD^{f-1}$$

4. *Improved (single fraction)*. This fourth strategy was designed to deliver each single fraction dose as close as possible to the TD. As such, all differences between the fraction wise DDs and the TD were considered separately.

$$TD^{f}_{improved\ SFD} = TD + (TD - DD^{1}) + (TD - DD^{2}) + (TD - DD^{3}) + \cdots = f \cdot TD - \sum_{i=1}^{f-1} DD^{i}$$

It is important to note that scenarios 2-4 can only be applied from the second fraction on. Additionally, the strategies *simple* and *improved (single fraction)* are conceptually very similar. Indeed, for the second fraction, they are identical. However, for the following fractions, the *improved (single fraction)* strategy provides a stronger modulation of the fraction specific TD, since the single fraction delivery deviations are considered separately.

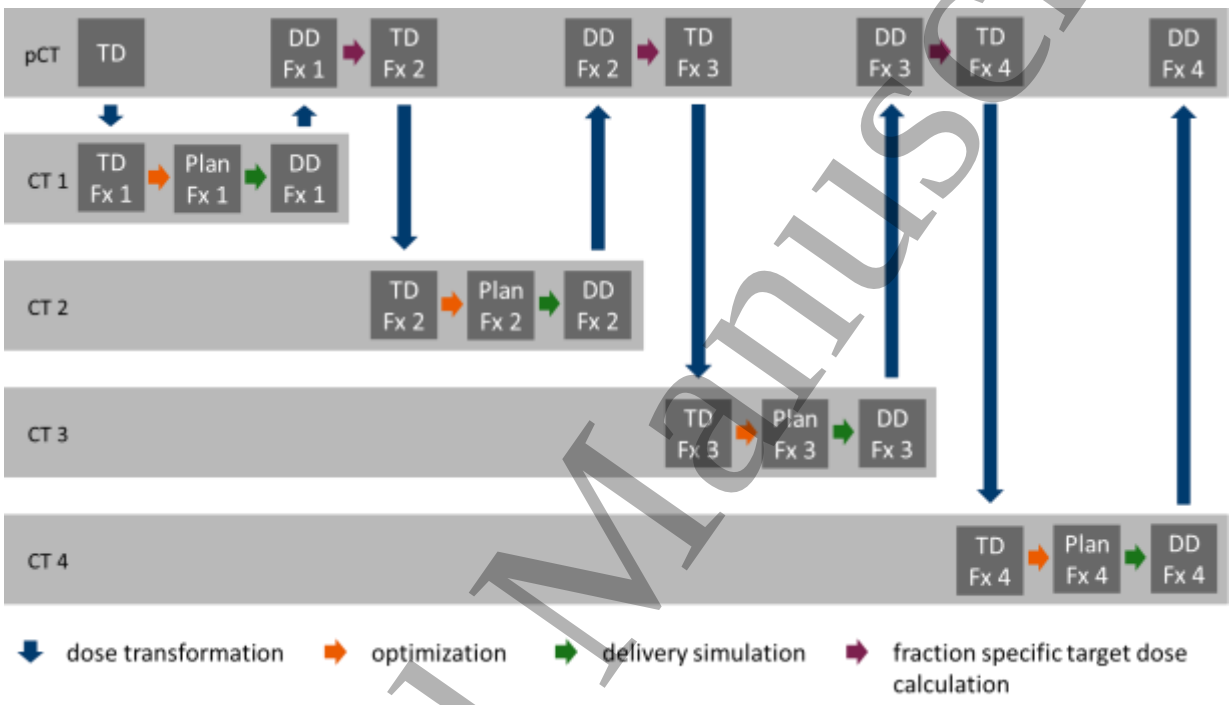

Figure 3 Schematic of patient planning study design. TD: target dose, DD: delivered dose (simulated)

2.1.2 Data analysis

We calculated 3D Gamma pass rates of the DDs and the ADs on the pCT compared to the initial TD for all four fractions. For the gamma evaluation the TD was chosen as a reference. A Gamma criterion of 1%/1 mm and 3%/1mm were chosen and only voxels with a dose above 10% of the prescribed dose were considered. Voxels in air were ignored.

2.2 Experimental validation with measurements

In a next step, we conducted dose measurements to investigate the UYD approach for correcting realistic delivery and calculational errors experimentally. For this, only the *simple* strategy was investigated, and just for two fractions. No anatomical or setup changes were considered.

2.2.1 Gantry and spot position accuracy

All measurements were performed on PSI gantry 2. This is a pencil beam-scanning gantry with upstream energy selection in the range 70–230 MeV, and a beam with between 2.5 and 4.5 mm σ in air(Pedroni *et al.*, 2004). Based on comprehensive analysis of machine log files, this machine has an

average positional accuracy in the placement of each pencil beam of about 0.5 mm (sigma), and is therefore comparable to the precision of commercial PBS machines(Toscano *et al.*, 2019). At our institute however, this is further improved clinically by applying spot specific positional offsets obtained from log-file analysis of a dry-run delivery of each field – a process called "teaching"(Bula, Meer and Pedroni, 2013). For the fields used for this experiment, average (max) spot position deviations were 0.27(0.65) and 0.14(0.95) mm in the two lateral scanning directions for untaught delivery, and 0.04(0.26) and 0.003(0.26) mm after teaching. Therefore, as we have two different delivery machine files for the same field (untaught and taught), each with different delivery accuracies, the effectiveness of UYD for correcting delivery errors has been tested with both, which will henceforth be referred to as *standard* (untaught) and *precise* (taught) delivery. Although this differentiation may seem somewhat academic, we aim to investigate whether a UYD paradigm can be used to compensate for a less precise delivery without the need of substantial improvements in delivery hardware or the use of processes such as teaching, which are incompatible with a daily adaptive approach.

2.2.2 Phantom and target dose plans

For the described experiments, we generated treatment plans for an anthropomorphic head phantom manufactured by CIRS (Computerized Imaging Reference Systems, Inc., Norfolk, VA, USA). A planning CT was obtained of one-half of the head (sagittal cut) placed on a PMMA spacer. This PMMA spacer served as a placeholder to extract the correct depth for comparison to the measurements. Two treatment plans consisting of one field were generated. The planning CT and the two treatment plans are shown in figure 4. Plan (a) consisted of a box shaped target. We chose the position of the box, such that the beam goes through the most heterogeneous part of the phantom and such that the interface between the phantom and the PMMA is in the middle of the target. Plan (b) consists of the same box, but additionally we chose two regions, one inside the box and one at the left edge of the box, where dose constraints were added. This resulted in a dose distribution with a hole in the middle of the box and a step in dose at the left edge. The plans were optimized with our in house developed TPS. The dose distributions from these treatment plans were considered the target dose distributions (TD) for the following experiments.

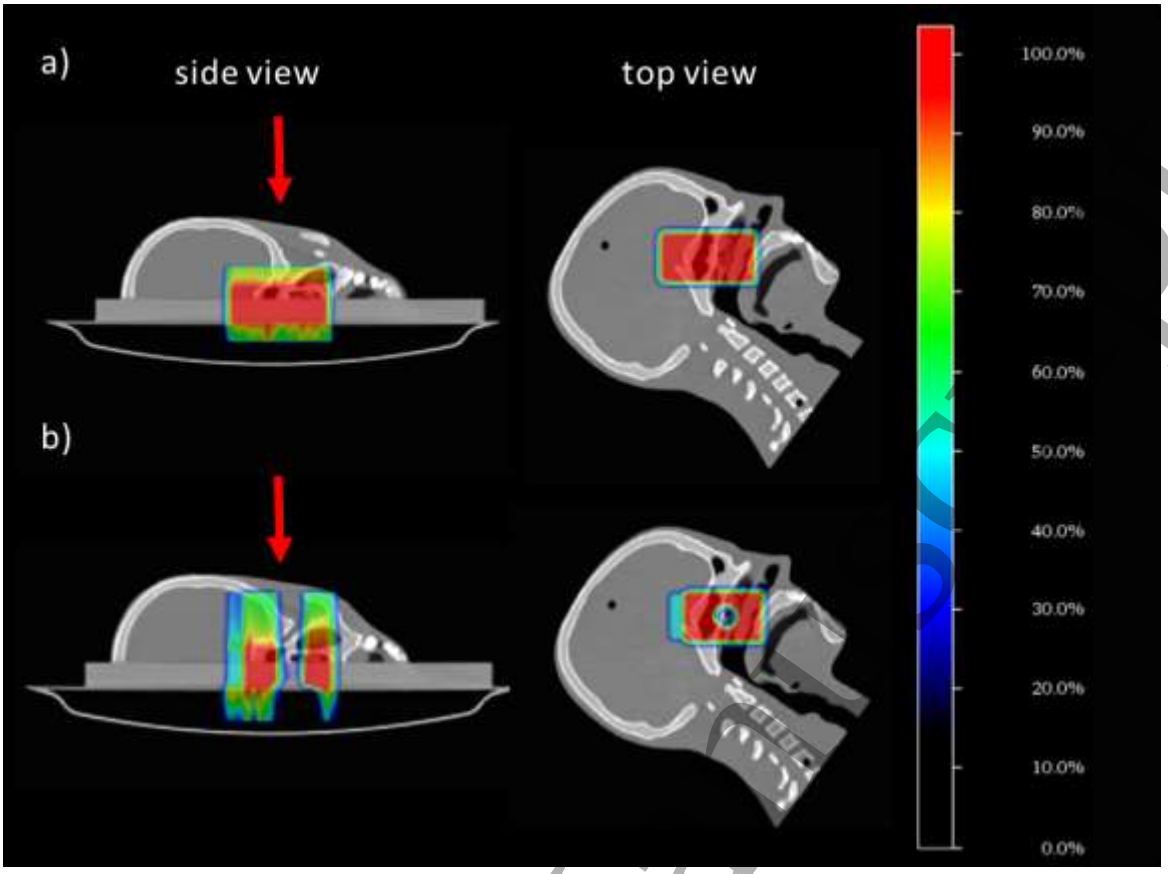

Figure 4 Planning CT of the half-head phantom with two box shaped target dose distributions. Target (a) is shown at the top and (b) at the bottom. The field direction is indicated with a red arrow. The color wash scale of the dose in % of the prescription is display on the right-hand side of the figure.

2.2.3 Measurement setup

We placed the half-head phantom on a scintillating screen, which is observed by a CCD camera under a mirror placed at an angle of 45° degrees (Boon *et al.*, 2000). The measurement setup is shown in figure 5. Both, the scintillating screen and the phantom were positioned with the help of the in room lasers. This way the center of the scintillating screen, the planned, as well as the actual field center were aligned. The read out of the CCD camera represented a relative 2D-dose measurement with a resolution of 0.4 mm. The measurement plane was 5 mm below the sagittal cut of the phantom. Therefore, we placed a PMMA spacer sheet below the half-head phantom for taking the planning CT. The screen showed some LET dependent quenching in the Bragg-peak region of up to 8% (Boon *et al.*, 1998), but by recalculating the dose distributions with quenching corrected depth-dose curves, we found that for our relative dose measurements quenching was negligible.

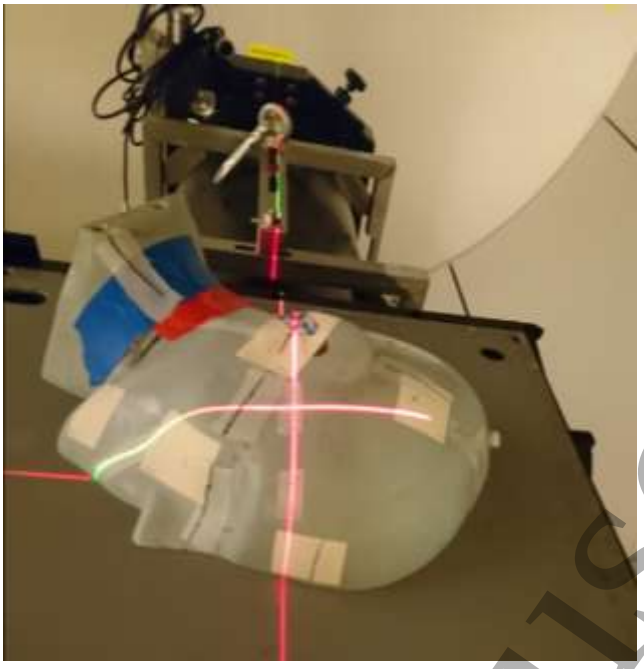

Figure 5 Half-head CIRS phantom positioned with laser alignment on the scintillating screen below gantry 2.

2.2.4 Log-files and Monte Carlo dose calculation

During the application of a field, the treatment control system measures various treatment machine parameters and records them into a log-file (Grossmann, 2007). For every spot, this information includes the measurement of the position in the transversal plane by strip monitors located in the gantry nozzle (Actis, Meer and König, 2014) and the proton fluence measured by two transmission chambers. The measurement of the spot position has an accuracy of 0.14 mm at the nozzle(Scandurra *et al.*, 2016). We used the information of the actual spot position and fluence for a dose calculation with the MC algorithm(Winterhalter, Meier, *et al.*, 2019). The resulting dose distribution is referred to as MCLog dose.

2.2.5 Experimental study design

Two different experiments have been conducted. Experiment 1 applied the *simple* update strategy to fraction 2. Experiment 2 aimed at correcting just for dose calculation algorithm differences in the first fraction, and additionally correcting for these and delivery errors in the second fraction. This second experiment was designed to test if the UYD method can already be applied to the first fraction, when no log-file is available yet. The update for the second fraction is then the same as for experiment 1. With Experiment 2 we could also investigate the effectiveness of UYD for correcting calculational and delivery errors separately.

2.2.6 Experiment 1: UYD for correcting both delivery and calculational errors

A schematic of the first experimental study design is shown in figure 6(a). A treatment plan for fraction 1 (Plan Fx 1) was optimized on the pCT with the initial target dose.

$$TD^{Fx\,1} = TD$$

The same optimization algorithm and settings as described for the simulation part (section 2.1.1) were used. Then the plan was delivered to the phantom, while measuring the 2D dose distribution below the phantom ($DD^{Fx\,1}$ measurement). During the delivery, a log-file was also recorded. The

delivered dose was reconstructed based on the log-file information with a MC algorithm ($DD^{Fx\,1\ MCLog}$). We calculated the TD for fraction 2 according to

$$TD^{Fx\,2} = TD + (TD - DD^{Fx\,1\ MCLog}).$$

This approach was analog to the strategy *simple*, as was described in section 2.1.1. Next, a fraction 2 plan (Plan Fx2) was optimized towards $TD^{Fx\,2}$, which was again delivered and measured (DD Fx 2 measurement).

2.2.7 Experiment 2: UYD with pre-correction for calculational errors in the first fraction

The second experiment addressed the problem that the procedure described in experiment 1 cannot be applied to the first fraction, because no feedback signal (log-file) is available from a previous fraction. However, if a MC simulation can be conducted before the first fraction delivery, one can use this information already for correction. We used the differences between a MC simulation and the analytically optimized plan as a feedback signal to already refine the first fraction delivery. This approach is analog to a method described by (Barragán Montero *et al.*, 2018). Figure 6 (b) shows a schematic of this procedure**.** In experiment 2, the Plan Fx 1 was at first recalculated with a MC algorithm (MC^{Fx1}). This MC dose distribution was used to calculate the first fraction target dose ($TD^{Fx\,1^*}$) according to

$$TD^{Fx\,1^*} = TD + (TD - MC^{Fx\,1}).$$

A renewed optimization resulted in the corrected first fraction plan (Plan Fx1*), which already considered calculational errors. Then this plan was delivered. Analog to experiment 1, the delivered dose was reconstructed based on the log-file information with a MC algorithm ($DD^{Fx\,1\,MCLog}$). The TD for fraction 2 was then calculated according to

$$TD^{Fx\,2} = TD + (TD - MC^{Fx\,1}) + (TD - DD^{Fx\,1\,MCLog}).$$

Here, the difference of the dose calculation *(TD-$MC^{Fx\,1}$)* and the differences from the first fraction delivery *(TD-$DD^{Fx\,1\ MCLog}$)* are considered separately. This approach is analog to the *improved (single fraction)* strategy in the simulation part of this study. The difference to the *improved (single fraction)* strategy used in the simulation was that the first dose distribution used for correction was a MC simulation only, without considering errors in the spot position.

We conducted all described measurements in both *standard* and *precise* delivery modes. For corrected deliveries, log-files obtained in the same mode were used for correction.

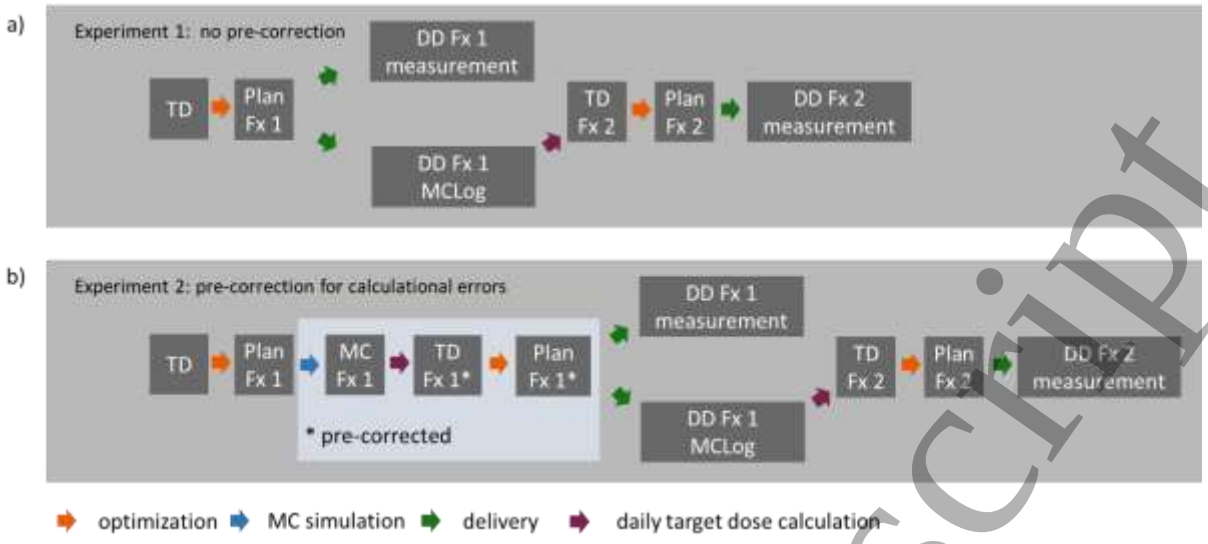

Figure 6(a) Schematic of experimental study design for experiment 1 and (b) for experiment 2. TD: target dose, DD: delivered dose, MC: Monte Carlo

2.2.8 Data analysis

In a first step, we extracted the 2D dose distribution of the calculations in the plane corresponding to the scintillating screen position. Then we interpolated the dose distribution to a grid corresponding to the CCD camera resolution. The lateral overlay was done by matching the planned field center to the center of the scintillating screen. The CCD camera measurements were background corrected. Both measurements and calculations were masked to exclude noise from the analysis in the no-dose area of the screen. The mask was chosen to be the area where the TD exceeded 0.5% of its maximal dose. Since it was a relative dose measurement, we normalized the measurement and the calculations. This was achieved by dividing both distributions, by the cumulative dose inside the masked area.

Lateral dose profiles of the measured and the calculated dose distributions were evaluated. All displayed profiles are along the x direction, which is from left to right in figure 4, at the field center. We also calculated 2D gamma test pass rates with criterion 1%/1mm of the two dose distributions. For the gamma evaluation points outside the masked area were ignored and the measured dose was used as a reference. Since the gamma test is sensitive to differences in noise levels of the compare data, additionally the root mean squared difference of the 2D dose distribution inside the masked area was evaluated. This evaluation was only done for the comparison of the agreement of the TPS and the log-file dose with the measurement.

3 Results

3.1 Simulations

The Gamma pass rate between the delivered dose simulations and the target dose for the single fractions are displayed in figure 7(a). For the first fraction, no correction was applied and therefore all strategies lie on the same point. For the second fraction, both the *simple* and the *improved (single fraction)* strategies show a clear improvement compared to the *no update* strategy. The *improved (accumulated)* strategy however, displays deterioration in the second fraction. In fraction 3 and 4, the *improved (single fraction)* strategy provided the best results. The results for the accumulated dose are shown in figure 7(b). Here, all update strategies show an improvement compared to the *no*

update strategy and, as would be expected, the *improved (accumulated dose)* strategy outperformed the others. As designed, the *improved (accumulated dose)* strategy manages to double correct for the delivery errors of the first fraction. This results in the deterioration in agreement of fraction 2 for the single fraction dose and the high agreement for the accumulated dose. Interestingly, the *improved (accumulated dose)* strategy already achieves a high agreement in the second fraction and no further improvement is observable.

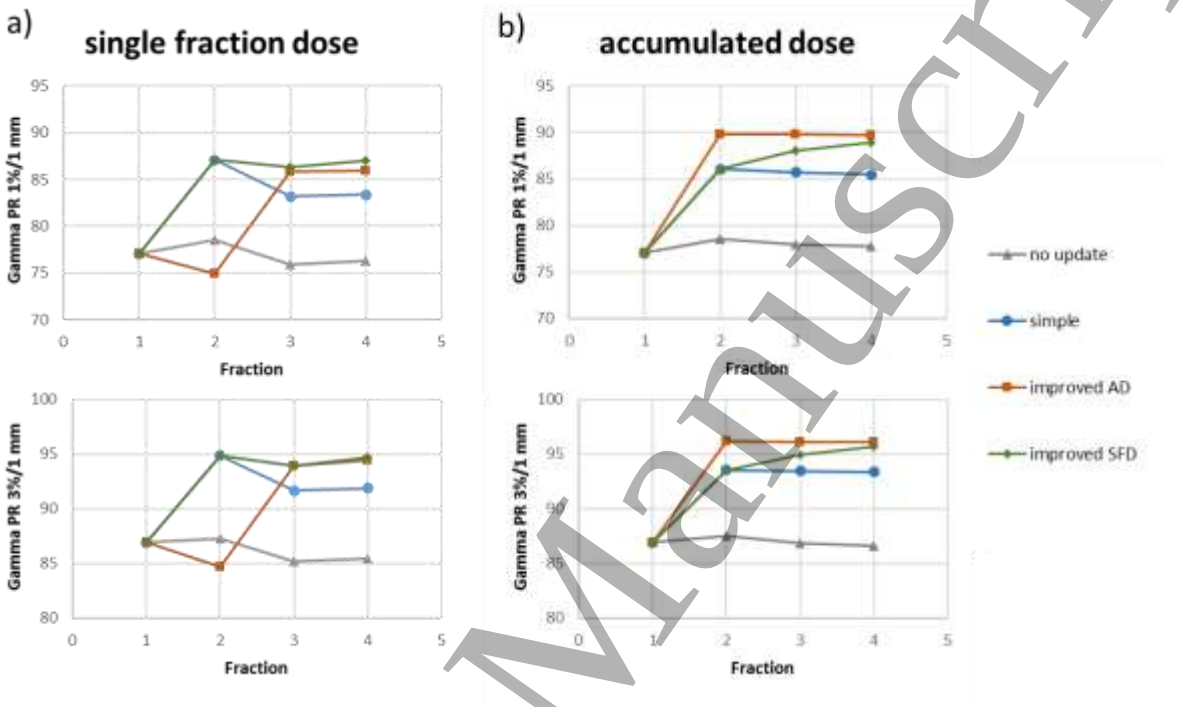

Figure 7 Gamma pass rate with criterion 1%/1 mm and 3%/1mm between the delivery simulations and the target dose. Single fraction doses are displayed in (a) and accumulated doses in (b). Four different strategies are compared: no update, ***simple****,* ***improved (accumulated)*** *and* ***improved (single fraction).***

3.2 Experimental validation

3.2.1 Agreement to measurement: TPS vs. MCLog dose

To legitimize the correction approach, we first need to show that the MC log-file calculations actually agree better to the measurement than the TPS dose. In figure 8, dose profiles are displayed for the first fraction treatment plan of the target doses (a) and (b) obtained in the *Standard* delivery mode. The measurement, the analytically calculated dose and the MCLog dose calculation are shown, all for the same delivery. The corresponding gamma pass rates are given in table 1 and the root mean squared voxel difference in table 2. In the profile display, it is clearly visible that the measurements agree very well with the calculations. Looking more closely however, one can also see that the MCLog dose corresponds better to the measurements than the TPS analytical dose. One place where this is clear, is in the dose hole in target (b), as the MC models secondary interactions more accurately than the analytical algorithm. The gamma pass rate and the root mean squared difference values clearly show the calculation accuracy improvement of the MCLog compared to the TPS dose

(table 1).

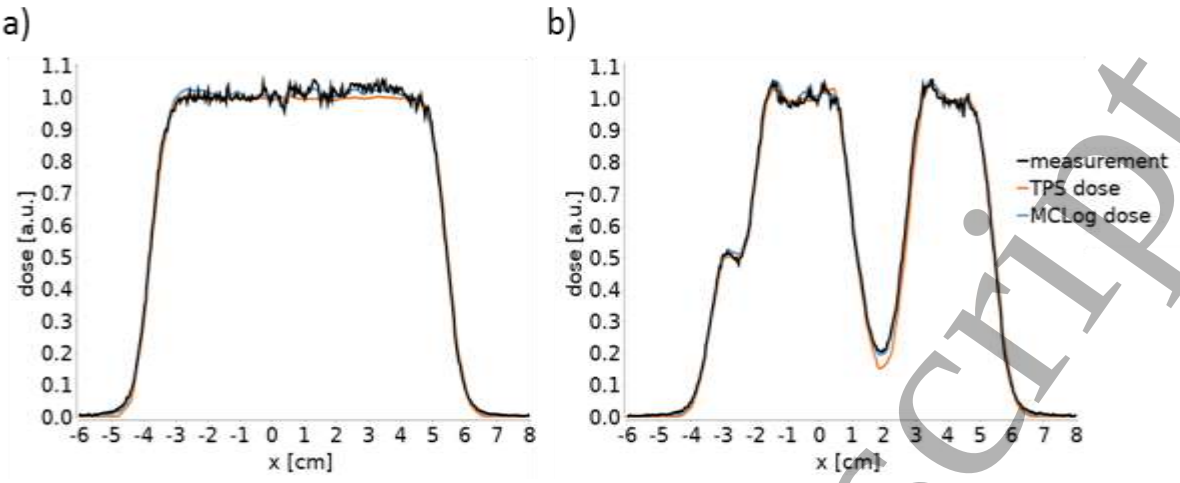

*Figure 8 Profiles of the measured and calculated dose distributions through the field center in the middle of the target. Target (a) is shown on the left and (b) on the right. The TPS-analytical dose is depicted in orange, the MCLog dose in blue and the CCD camera measurement in black. The measurements were obtained in the **standard spot position delivery** mode and all dose profiles were normalized.*

*Table 1 Agreement between the TPS-analytical dose with the measurement and the MCLog dose with the measurement for target (a) and (b). Comparison metric is Gamma pass rate (1%/1mm). The measurements were obtained in the **standard spot position delivery** mode.*

Gamma PR [%] of comparison between measurement and	Target a)	Target b)
TPS-analytical dose	74.67	73.24
MCLog dose	99.43	99.25

*Table 2 Agreement between the TPS-analytical dose with the measurement and the MCLog dose with the measurement for target (a) and (b). Comparison metric is root mean squared voxel difference. The measurements were obtained in the **standard spot position delivery** mode.*

Root mean squared voxel difference [a.u.] between measurement and	Target a)	Target b)
TPS-analytical dose	0.032	0.032
MCLog dose	0.016	0.015

3.2.2 Experiment 1: UYD for correcting both delivery and calculational errors

The dose profiles for the first and second fraction obtained in the *standard* delivery mode are shown in figure 9 for both targets (a) and (b). Especially in the dose hole of target (b), the increase of agreement between the measurement and the target dose for the second fraction can be observed. The gamma pass rate for the first and second fraction for both spot position delivery modes and both targets are shown in figure 10. In every case the second fraction, where the corrections were applied, displays a better agreement to the TD than the first fraction, and a similar agreement between measurements and TD for both targets can be observed. In addition, although the agreement to the TD at the second fraction is not quite as good for the *standard* compared to *precise* delivery mode, these results demonstrate that a UYD approach can nevertheless substantially compensate for the larger imprecisions in delivery.

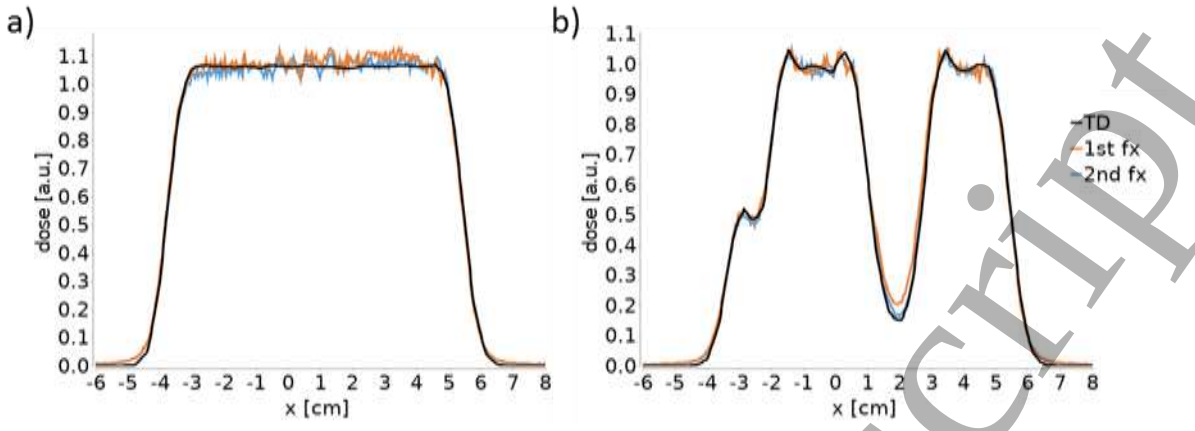

*Figure 9 Profiles of the measurements of the first (orange) and second fraction (blue) compared to the TD (black) for both targets (a) and (b). The profiles through the field center in the middle of the target are displayed. The measurements were obtained in the **standard spot position delivery** mode and all dose profiles were normalized.*

*Figure 10 Gamma pass rate for the measurements of the first and second fraction and both targets for the **standard** and **precise spot position delivery** mode.*

3.2.3 Experiment 2: UYD with pre-correction for calculational errors in the first fraction

Gamma pass rates for the first and second fraction in *standard* and *precise* delivery mode are shown for both targets in figure 11 with correction of the first fraction for calculational errors. A higher agreement to the target dose compared to the case without the additional correction step (experiment 1) is clearly observed for the first fraction. Indeed, in particular for the *precise* delivery, the first fraction already shows high Gamma pass rates (around 90%). Nevertheless, an additional small improvement could be achieved in the second fraction due to the additional feedback of delivery errors to the optimizer. The pass rates of the second fractions are comparable to the ones without the additional correction step (experiment 1).

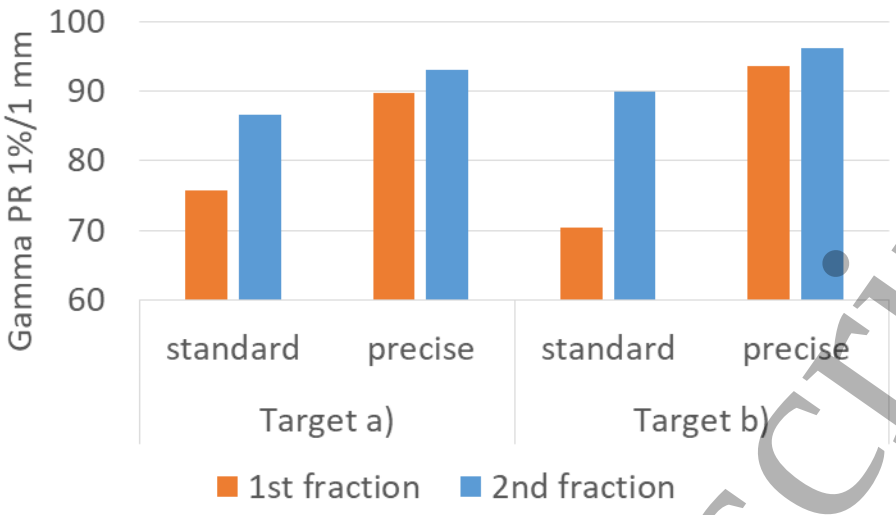

*Figure 11 Gamma pass rate for the measurements of the first and second fraction and both targets with an additional correction for calculational errors of the firs fraction for the **standard** and **precise spot position delivery** mode.*

4 Discussion

With the fractionated daily adapted treatment simulation, we showed that a feedback signal in the form of a dose distribution is useful to refine a DAPT delivery. First, we applied the closed-loop process in a DAPT scenario, where every fraction is delivered to a new CT. The UYD method enabled a clear reduction of differences between the delivered and the intended target dose. Further, we investigated different strategies to incorporate the dose feedback signal, which displayed the expected behavior. Second, the measurements showed that the simulated improvements of UYD could be transferred to a real delivery machine. We could achieve an improved agreement between the measured dose and the intended dose for the second fraction, when using the information from the log-file of the first fraction delivery. The improvements of UYD are in the same order of magnitude for both, the simulations and the measurements. Therefore, we believe UYD is a promising candidate for refining the delivery of DAPT.

To start the discussion, let us examine the feedback signal used for UYD. It is a dose distribution coming from a log-file MC simulation. This dose distribution corresponds better to what is actually delivered than the planned dose in two aspects. First, it uses measured values for spot position and fluence and not planned values. Second, it uses a precise, but calculation time intensive, MC simulation and not the fast analytical dose calculation algorithm. Of course, correcting for delivery errors with the information available in the log-file is only a valid approach, as long as the measured information in the log-file is accurate. These values however, can be highly inaccurate as was pointed out by (Toscano *et al.*, 2019). Thus, their accuracy needs to be carefully checked and validated by each institute. In the results section 3.2.1 we show that the MCLog dose agrees better to the measurement than our TPS dose. Of course, this effect has two possible explanations, the additional information in the log-file and the more accurate dose calculation. Both explanations contribute to the accuracy improvement. This is shown by experiment 2 (pre-correction for calculational errors of the first fraction), since correcting for the dose algorithm errors separately resulted in an improved agreement and then additional correction for the delivery errors further

improved the situation (fig. 10). The UYD method worked for both the *standard* and the *precise* delivery mode. But, as expected, the improvement due to UYD was bigger for the *standard* delivery mode, since there were larger delivery errors which could be corrected for. The spot position error has a systematic (same for the repeated delivery of the same plan) and a random component. While the correction for the systematic component with UYD is easy to understand, UYD also works for random spot position errors. This is shown by the simulation study, where only random spot position errors were simulated. A possible explanation for this is that also random spot position errors have a predictable effect on the resulting dose distribution, mainly a smearing out effect. Finally, we believe that our approach for the correction of delivery errors is also applicable for other commercial systems, since commercial proton therapy machines have an accuracy of spot positioning which roughly corresponds to the *standard* delivery mode(Toscano *et al.*, 2019).

The other component of the feedback signal is the accurate MC dose calculation. Correcting for inaccuracies of the analytical dose calculation is only possible if a better dose calculation engine is available. Obviously, it would be best to base the plan optimization on an accurate MC simulation. But, in some cases no MC calculation is available in the used TPS or an accurate MC simulation would take too much calculation time, as could be the case for an online adaption application. Here, we describe another way to incorporate the information from a time intensive, but accurate, dose calculation and we could show, that inaccuracies from a simple dose calculation for the optimization can be corrected for. Interestingly, the correction method is valid even though the optimization of the plan incorporating the correction is still based on an analytical algorithm. We believe that especially for DAPT, where a MC based optimization is not always possible due to time limitations, UYD might bring a big benefit.

The UYD method could also be used in a non-DAPT (standard) treatment approach, where the patient is treated with a plan optimized on the planning CT over the whole treatment. The drawback is that the positioning uncertainty could destroy the benefit from UYD. For example, if during fraction n a certain spot position error causes a hot and a cold spot, there is no guarantee that in fraction n+1 the patient lies exactly at the same position. Therefore, correcting for yesterday's hot and cold spot in the new daily anatomy could result in a deterioration of the applied dose. If the treatment is not planned on the daily patient geometry, we believe one should not correct for delivery or algorithm errors of the previous fractions, but try to deliver a treatment goal-satisfying dose every day.

If the UYD method is applied in a DAPT treatment approach, patient positioning uncertainties or anatomical changes are considered during the optimization. Of course, the problem of intra-fraction motion remains, but this is for most sites much smaller than inter-fraction motion. However, for UYD a new problem arises: Dose accumulation. Dose accumulation relies on a registration, between the daily CTs and a reference CT. This is highly problematic in anatomical regions where deformations occur. This is a widely discussed problem and much research is conducted to tackle that problem(Oh and Kim, 2017; Chetty and Rosu-Bubulac, 2019). In other regions, as for example the head, no deformations are expected and a rigid registration is a valid approach for dose accumulation. But even for the rigid case, a registration uncertainty is present, which affects the resulting dose accumulation. However, in this treatment simulation study, we could observe a clear improvement with the UYD method despite uncertainties in the rigid registration. Nevertheless, the extension of

the proposed method to anatomical regions where deformations occur is currently discouraged, unless a reliable deformable image registration is available.

In this study, we followed the re-optimization approach of dose restoration. There are different advantages and disadvantages of this approach, which are thoroughly discussed elsewhere(Bernatowicz *et al.*, 2018; Matter *et al.*, 2019). We chose this approach, as a showcase to illustrate the validity of the UYD approach. Indeed, it is easier to compare the delivered dose to a target dose rather than comparing dose volume constraints. When using an optimization towards the same target dose every day, it is straightforward to evaluate and compare agreement towards this target dose. For optimization towards pre-defined dose volume constraints, the situation is much more difficult, since every correction is a trade-off between competing constraints. However, the UYD method is expected to work also for other re-optimization approaches, even if possibly the improvements might be more hidden.

In the fractionated DAPT treatment simulation, we investigated different strategies to incorporate yesterday's dose. The *simple update* strategy was the most straightforward approach. The *improved (accumulated)* or the *improved (single fraction)* strategies represented a stronger correction modulation. Therefore, one can say that they represent more aggressive correction approaches, which resulted in a better agreement between the delivered dose and the target dose. It is difficult to assess which strategy is better, refining the single fraction doses or the accumulated dose. To address this question properly the biological effect of the fractionation scheme would need to be considered. Anyhow, in the examined example both strategies converged to the same agreement between delivered and target dose after the third fraction for both the single fraction and the accumulated dose.

Regarding the *pre- correction for calculational errors* method from the measurements (experiment 2), one can argue that in a fractionated treatment the additional correction of the first fraction does not make a big difference. In a hypo-fractionated treatment however, getting the dose right at the first fraction already, might be more important. Another option to refine the first fraction delivery would be to conduct a dry-run delivery before and then use the log-file from this dry-run to apply the correction. Nevertheless, *pre-correction for calculational errors* is useful, if a dry-run is not feasible and this experiment 2 gave an interesting inside in how strong the relative effects of delivery and dose calculation errors are.

Finally, in this paper, dose distributions have been compared using the Gamma-index method. We made this choice, because it is the most common test, even though the Gamma pass rate test is sensitive to the noise level of the investigated data (Cohilis *et al.*, 2020). In this case, both the measurement data and the MC calculation data have a non-negligible level of noise. However, when comparing the same kind of dose distribution for the first and the second fraction, the relative change in Gamma pass rate is not affected by different noise levels. The only place where noise could invalidate our results is the comparison between the MCLog and the TPS dose calculation with the measurements (Section 3.2.1). Although our MCLog dose calculations have a noise level of below 1%, the Gamma pass rate of the MCLog dose with the measurement could nevertheless be over-estimated. However, the improved agreement of the MCLog dose with the measurement is also displayed by the root mean squared difference. The difference to the measurement for the MCLog dose is about half than for the TPS dose (table 2).

However, a word of caution is appropriate. Any deviations between the dose distribution used as a feedback signal and the actual dose, which is delivered in the patient, can cause a deterioration of the initial plan, if it is used for correction. If these deviations are of a systematic nature, this means that a similar deviation appears at the same position over multiple fractions, then the adapted plan iteratively deteriorates. There are many reasons for such deviations, as for example errors in the registration, faulty log-files or shortcomings of the MC algorithm. If UYD would be applied in patient treatments, a threshold would need to be defined on the amount of adaption away from the original plan that is allowed. This would prevent an uncontrolled divergence of the corrected plan away from the initial dose. A safer way might be an off-line optimization goal update. After a couple of fractions the accumulated dose can be visually checked and, if there are undesired dose effects, the optimization goal for the remaining fractions altered accordingly. As Yan et al. have already pointed out, the closed-loop process can be extended to further measurement modalities(Yan *et al.*, 1997) that might make for a safer process. For this, a high-resolution in-vivo dose measurement would be ideal as a compliment to the log-file based MC calculations used in this work.

5 Conclusion

A proof of concept for a closed-loop adaption process, with a log-file MC dose calculation as a feedback, has been described. The method has been shown to refine the daily adapted proton delivery by correcting for delivery errors and inaccuracies of the dose calculation algorithm used for optimization. This has been demonstrated with both simulated DAPT treatments, and measurements using an anthropomorphic phantom.

Acknowledgment

This publication was formed in the scope of the Swiss national science foundation project ‘Towards the Daily Adapted Proton Therapy at PSI’. The authors would like to acknowledge SNF for their support with the grant SNF: 320030_165961.

6 Bibliography

Acharya, S. *et al.* (2016) ‘Online Magnetic Resonance Image Guided Adaptive Radiation Therapy: First Clinical Applications Radiation Oncology’, *Int J Radiation Oncol Biol Phys*, 94(2), pp. 394–403. doi: 10.1016/j.ijrobp.2015.10.015.

Actis, O., Meer, D. and König, S. (2014) ‘Precise on-line position measurement for particle therapy’, in *Journal of Instrumentation*. doi: 10.1088/1748-0221/9/12/C12037.

Albertini, F. *et al.* (2008) ‘Sensitivity of intensity modulated proton therapy plans to changes in patient weight.’, *Radiotherapy and oncology : journal of the European Society for Therapeutic Radiology and Oncology*, 86(2), pp. 187–94. doi: 10.1016/j.radonc.2007.11.032.

Albertini, F. *et al.* (2020) ‘Online daily adaptive proton therapy’, *The British journal of radiology*, 93(1107), p. 20190594. doi: 10.1259/bjr.20190594.

Barragán Montero, A. M. *et al.* (2018) ‘Performance of a hybrid Monte Carlo-Pencil Beam dose algorithm for proton therapy inverse planning’, *Medical Physics*. Wiley-Blackwell, 45(2), pp. 846–

862. doi: 10.1002/mp.12688.

Bernatowicz, K. *et al.* (2018) 'Feasibility of online IMPT adaptation using fast, automatic and robust dose restoration', *Physics in Medicine & Biology*. IOP Publishing, 63(8), p. 085018. doi: 10.1088/1361-6560/aaba8c.

Bohoudi, O. *et al.* (2017) 'MRI-guided radiotherapy Fast and robust online adaptive planning in stereotactic MR-guided adaptive radiation therapy (SMART) for pancreatic cancer', *Radiotherapy and Oncology*, 125, pp. 439–444. doi: 10.1016/j.radonc.2017.07.028.

Boon, S. N. *et al.* (1998) 'Fast 2D phantom dosimetry for scanning proton beams', *Medical Physics*. doi: 10.1118/1.598221.

Boon, S. N. *et al.* (2000) 'Performance of a fluorescent screen and CCD camera as a two-dimensional dosimetry system for dynamic treatment techniques', *Medical Physics*, 27(10), pp. 2198–2208. doi: 10.1118/1.1289372.

Botas, P. *et al.* (2018) 'Online adaption approaches for intensity modulated proton therapy for head and neck patients based on cone beam CTs and Monte Carlo simulations', *Physics in Medicine & Biology*. IOP Publishing, 64(1), p. 015004. doi: 10.1088/1361-6560/aaf30b.

Bula, C., Meer, D. and Pedroni, E. (2013) 'System for the delivery of proton therapy by pencil beam scanning of a predeterminable volume within a patient'. United States.

Chetty, I. J. and Rosu-Bubulac, M. (2019) 'Deformable Registration for Dose Accumulation', *Seminars in Radiation Oncology*, 29(3), pp. 198–208. doi: 10.1016/j.semradonc.2019.02.002.

Cohilis, M. *et al.* (2020) 'A noise correction of the γ-index method for Monte Carlo dose distribution comparison', *Medical Physics*. doi: 10.1002/mp.13888.

Grossmann, M. (2007) 'Cancer Therapy with Protons at Paul Scherrer Institut', in *2007 15th IEEE-NPSS Real-Time Conference*. IEEE, pp. 1–3. doi: 10.1109/RTC.2007.4382765.

Hoffmann, L. *et al.* (2017) 'Adaptation is mandatory for intensity modulated proton therapy of advanced lung cancer to ensure target coverage', *Radiotherapy and Oncology*, 122(3), pp. 400–405. doi: 10.1016/j.radonc.2016.12.018.

Jagt, T. *et al.* (2017) 'Near real-time automated dose restoration in IMPT to compensate for daily tissue density variations in prostate cancer', *Physics in Medicine and Biology*. doi: 10.1088/1361-6560/aa5c12.

Kontaxis, C. *et al.* (2015) 'A new methodology for inter-and intrafraction plan adaptation for the MR-linac', *Physics in Medicine & Biology Phys. Med. Biol*, 60, pp. 7485–7497. doi: 10.1088/0031-9155/60/19/7485.

Lomax, J. A. *et al.* (1996) 'A 3D treatment planning for conformal proton therapy by spot scanning. Quantitative Imaging in Oncology'. Available at: https://www.scienceopen.com/document?vid=3e3a597b-4c23-45c6-853a-7511022d3a34 (Accessed: 18 December 2017).

Matter, M. *et al.* (2019) 'Intensity modulated proton therapy plan generation in under ten seconds', *Acta Oncologica*. doi: 10.1080/0284186X.2019.1630753.

Nenoff, L. *et al.* (2019) 'Daily adaptive proton therapy–the key to innovative planning approaches for paranasal cancer treatments', *Acta Oncologica*. doi: 10.1080/0284186X.2019.1641217.

Nenoff, L. *et al.* (2020) 'Daily adaptive proton therapy: Is it appropriate to use analytical dose calculations for plan adaption?', *International Journal of Radiation Oncology, Biology, Physics*, (accepted for publication).

Nijkamp, J. *et al.* (2012) 'Adaptive radiotherapy for long course neo-adjuvant treatment of rectal cancer', *Radiotherapy and Oncology*. doi: 10.1016/j.radonc.2012.02.013.

Oh, S. and Kim, S. (2017) 'Deformable image registration in radiation therapy', *Radiation Oncology Journal*. Korean Society for Therapeutic Radiology and Oncology, 35(2), p. 101. doi: 10.3857/ROJ.2017.00325.

Pedroni, E. *et al.* (2004) 'The PSI Gantry 2: A second generation proton scanning gantry', *Zeitschrift fur Medizinische Physik*. doi: 10.1078/0939-3889-00194.

Perl, J. *et al.* (2012) 'TOPAS: An innovative proton Monte Carlo platform for research and clinical applications', *Medical Physics*. John Wiley & Sons, Ltd, 39(11), pp. 6818–6837. doi: 10.1118/1.4758060.

Raaymakers, B. W. *et al.* (2017) 'First patients treated with a 1.5 T MRI-Linac: clinical proof of concept of a high-precision, high-field MRI guided radiotherapy treatment', *Physics in Medicine & Biology*. IOP Publishing, 62(23), pp. L41–L50. doi: 10.1088/1361-6560/aa9517.

Scandurra, D. *et al.* (2016) 'Assessing the quality of proton PBS treatment delivery using machine log files: Comprehensive analysis of clinical treatments delivered at PSI Gantry 2', *Physics in Medicine and Biology*. doi: 10.1088/0031-9155/61/3/1171.

Toscano, S. *et al.* (2019) 'Impact of machine log-files uncertainties on the quality assurance of proton pencil beam scanning treatment delivery', *Physics in Medicine and Biology*, 64(9). doi: 10.1088/1361-6560/ab120c.

Winterhalter, C., Zepter, S., *et al.* (2019) 'Evaluation of the ray-casting analytical algorithm for pencil beam scanning proton therapy', *Physics in Medicine and Biology*. doi: 10.1088/1361-6560/aafe58.

Winterhalter, C., Meier, G., *et al.* (2019) 'Log file based Monte Carlo calculations for proton pencil beam scanning therapy', *Physics in Medicine and Biology*. doi: 10.1088/1361-6560/aaf82d.

Yan, D. *et al.* (1997) 'Adaptive radiation therapy', *Physics in Medicine and Biology*, 42(1), pp. 123–132. doi: 10.1088/0031-9155/42/1/008.

Yan, D. *et al.* (2000) 'An off-line strategy for constructing a patient-specific planning target volume in adaptive treatment process for prostate cancer', *International Journal of Radiation Oncology Biology Physics*. doi: 10.1016/S0360-3016(00)00608-8.